J Nanostruct 16(3): 3112-3125, Summer 2026

RESEARCH PAPER

Kinetic Modelling and pH-Dependent Adsorption of Malachite Green onto Pectin/Poly(NIPAm-co-Acrylic Acid) Nano-hydrogel: Mechanistic Insights

Sajid S. Abbas [1], *Layth S. Jasim* [2]*

[1] *Ministry of Education General Directorate of Al-Qadisiyah Education, Diwaniyah, Iraq*

[2] *Department of Chemistry, College of Education, University of Al-Qadisiyah, Diwaniyah, Iraq*

ARTICLE INFO

Article History:
Received 28 February 2026
Accepted 13 May 2026
Published 01 July 2026

Keywords:
Adsorption kinetics
Malachite green
Nano-hydrogel
Pectin nano-hydrogel
Point of zero charge
Pseudo-second-order

ABSTRACT

The present work investigates the adsorption kinetics and pH-responsive behaviour of malachite green (MG) dye onto a novel pectin/poly(N-isopropylacrylamide-co-acrylic acid) nano-hydrogel synthesized via free-radical copolymerization. The nano-hydrogel was characterized using Fourier-transform infrared spectroscopy (FTIR), X-ray diffraction (XRD), scanning electron microscopy (FE-SEM), thermogravimetric analysis (TGA), and BET surface area measurements. Batch adsorption experiments were conducted to evaluate the effects of adsorbent dosage (0.006–0.06 g), contact time (1–150 min), and solution pH (2–10) on MG removal efficiency. The optimum adsorbent weight was found to be 0.008 g, yielding an adsorption capacity of 596.04 mg/g with 95.37% removal efficiency. Kinetic analysis revealed that the pseudo-second-order model provided the best fit ($R^2 \approx 1.000$; RMSE = 0.89 mg/g) with a calculated equilibrium capacity of 605.13 mg/g, suggesting chemisorption as the rate-controlling mechanism. The Weber–Morris intraparticle diffusion model indicated a two-stage process involving rapid surface adsorption followed by gradual pore diffusion. The point of zero charge (pH_{PZC}) was determined at pH 4.2, explaining the enhanced adsorption capacity observed at higher pH values where the surface acquires a net negative charge. MG adsorption increased from 515.21 mg/g at pH 2 to 608.96 mg/g at pH 10, confirming electrostatic attraction as a dominant mechanism. Regeneration studies demonstrated that the nano-hydrogel retained 87.8% of its initial adsorption capacity after five adsorption–desorption cycles using 0.1 M HCl/50% ethanol eluent. Furthermore, the adsorbent maintained >79% removal efficiency in simulated industrial wastewater containing competing ions and organic co-contaminants.

How to cite this article
Abbas S. Jasim L. Kinetic Modelling and pH-Dependent Adsorption of Malachite Green onto Pectin/Poly(NIPAm-co-Acrylic Acid) Nano-hydrogel: Mechanistic Insights. J Nanostruct, 2026; 16(3):3112-3125. DOI: 10.22052/JNS.2026.03.008

INTRODUCTION

Water contamination by synthetic dyes from textile, paper, and leather industries has become a pressing environmental concern worldwide. Among these pollutants, malachite green (MG), a triphenylmethane cationic dye, is extensively used in dyeing processes, aquaculture, and as an antifungal agent. Despite its wide application, MG

* *Corresponding Author Email: layth.jasim@qu.edu.iq*

poses serious health risks including carcinogenicity, mutagenicity, and respiratory toxicity, even at low concentrations [1,2]. Its molecular stability and resistance to natural degradation necessitate the development of effective remediation strategies. Several techniques have been explored for dye removal from wastewater, including photocatalytic degradation, coagulation, membrane filtration, and biological treatment [3,4]. Nevertheless, adsorption has gained considerable attention due to its operational simplicity, cost-effectiveness, and high removal efficiency across a broad spectrum of pollutant concentrations [5,6].

Hydrogel-based adsorbents have emerged as promising candidates owing to their three-dimensional cross-linked polymer networks, tuneable swelling capacity, and abundant functional groups that facilitate pollutant binding [7,8]. Stimuli-responsive hydrogels, in particular those incorporating poly(N-isopropylacrylamide) (PNIPAm) and pH-sensitive monomers such as acrylic acid, exhibit dual responsiveness to temperature and pH changes, which can be exploited to enhance adsorption performance and enable regeneration under controlled conditions [9,10]. The incorporation of natural polysaccharides like pectin into the hydrogel matrix further improves biocompatibility, hydrophilicity, and the density of carboxyl functional groups available for electrostatic interaction with cationic pollutants [11,12].

Despite the considerable progress made in hydrogel-based adsorption, detailed kinetic and pH-dependent mechanistic studies on pectin-based multi-responsive hydrogels for MG removal remain scarce. Most existing studies either focus solely on equilibrium data or employ single-component hydrogels lacking the synergistic benefits of combined natural and synthetic polymers [13,14]. This study therefore aims to synthesize a pectin/poly(NIPAm-co-acrylic acid) nano-hydrogel through free-radical copolymerization and to systematically investigate the kinetic behaviour and pH-dependent adsorption mechanism for MG dye. Particular attention is given to determining the rate-controlling step via pseudo-first-order, pseudo-second-order, and Weber–Morris diffusion models, alongside elucidating the role of surface charge through point of zero charge analysis. The findings presented herein contribute to a deeper understanding of structure–performance relationships in multi-responsive hydrogels and offer practical insights for designing efficient adsorbents for cationic dye removal.

MATERIALS AND METHODS

Materials

Pectin (from citrus peel), N-isopropylacrylamide (NIPAm, 97%), acrylic acid (AA, 99%), N,N'-methylenebisacrylamide (MBA, cross-linking agent), and potassium persulphate (KPS, initiator) were purchased from Sigma-Aldrich and used without further purification. Malachite green oxalate ($C_{23}H_{25}ClN_2$, molecular weight 364.91 g/mol, λmax = 621.6 nm) was obtained from Merck. Hydrochloric acid (HCl, 1 M) and sodium hydroxide (NaOH, 1 M) were employed for pH adjustment. Sodium chloride (NaCl, 0.1 M) was used in point of zero charge determination. All solutions were prepared using deionized water.

Synthesis of Pectin/Poly(NIPAm-co-Acrylic Acid) Nano-hydrogel

The nano-hydrogel was synthesized through free-radical copolymerization in aqueous solution. Briefly, 0.5 g of pectin was dissolved in 30 mL of deionized water under continuous stirring at 40°C. After 30 min, 0.4 g of NIPAm was added to the solution with stirring, followed by the addition of 4 mL of acrylic acid after 15 min. Subsequently, 0.04 g of MBA (cross-linker) dissolved in 2 mL of deionized water was introduced into the mixture under nitrogen atmosphere. In a separate vessel, 0.04 g of KPS (initiator) was dissolved in 2 mL of water and then added to the reaction mixture while maintaining nitrogen purging and continuous stirring at 40°C. The resulting pre-gel solution was transferred into glass tubes and placed in a water bath at 70°C for 6 h to complete the polymerization. The obtained nano-hydrogel was cut into small pieces, washed repeatedly with deionized water (replacing water every 60 min) to remove unreacted monomers and oligomers, and subsequently dried in an oven at 70°C for 48 h until a constant weight was achieved. The dried nano-hydrogel was finely ground and sieved through a 100 µm mesh for subsequent adsorption experiments. The gel content was determined gravimetrically and found to be 93.23%, confirming a high degree of cross-linking.

Characterization Techniques

The functional groups of the synthesized nano-hydrogel were identified by Fourier-transform

infrared spectroscopy (FTIR, Shimadzu 8400S) in the range 400–4000 cm^{-1} using KBr pellets. The crystalline structure was analysed by X-ray diffraction (XRD, Shimadzu XRD-6000) with Cu-Kα radiation (λ = 1.5406 Å) over 2θ range of 5–80°. Surface morphology was examined using field-emission scanning electron microscopy (FE-SEM, TESCAN MIRA3) at 20 kV accelerating voltage. Thermal stability was assessed by thermogravimetric analysis (TGA, Perkin Elmer TGA4000) from 30 to 750°C at a heating rate of 10°C/min under nitrogen atmosphere. BET surface area and pore size distribution were determined by nitrogen adsorption–desorption isotherm at 77 K (Quantachrome NOVA 2200e).

Point of Zero Charge Determination

The point of zero charge (pH_{PZC}) was determined

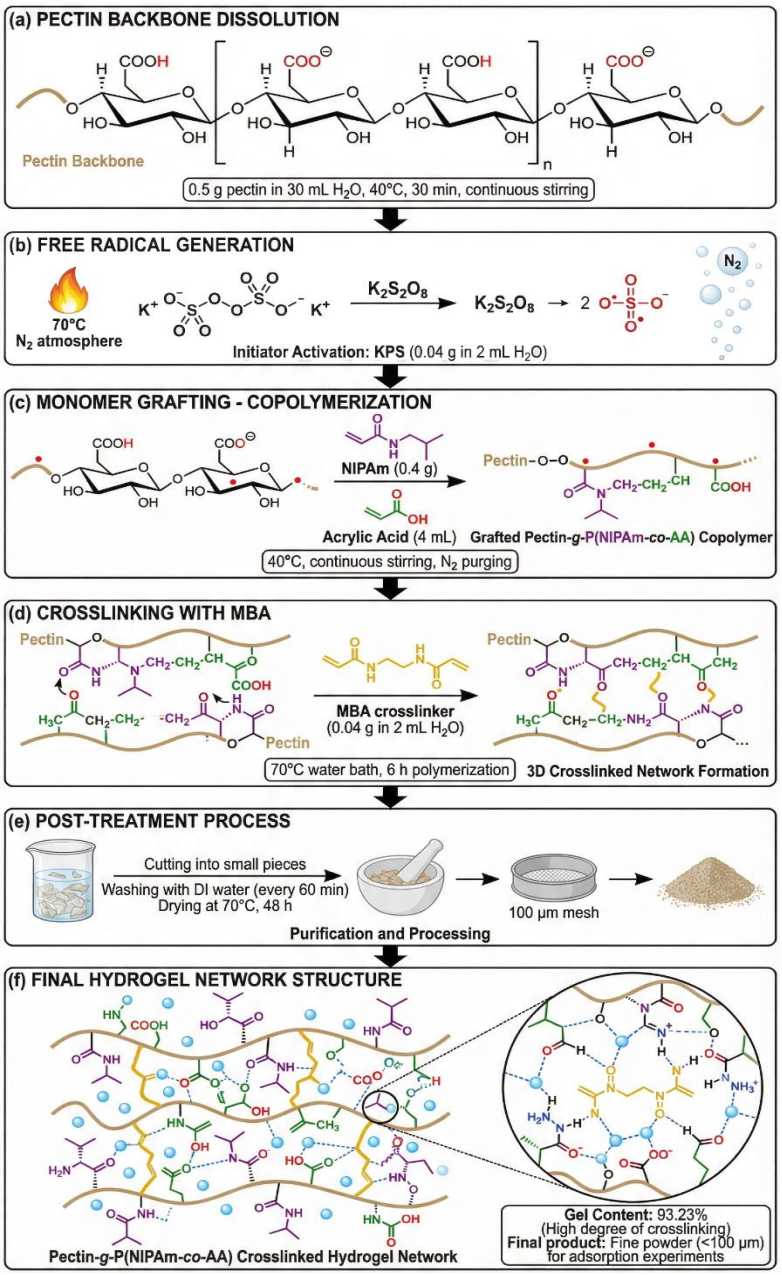

Fig. 1. Schematic illustration of the stepwise synthesis of Pectin-g-P(NIPAm-co-AA).

using the pH drift method. A mass of 0.02 g of the nano-hydrogel was added to 25 mL of 0.1 M NaCl solution at various initial pH values (pH_i = 2–12), adjusted using 1 M HCl or NaOH. The suspensions were agitated at 120 rpm for 24 h at 25°C. The final pH (pH_f) was measured, and ΔpH (= pH_f – pH_i) was plotted against pH_i. The pH_{PZC} corresponds to the pH_i at which ΔpH = 0 [15].

Batch Adsorption Experiments

All adsorption experiments were performed in batch mode. A stock solution of MG (1000 mg/L) was prepared by dissolving 1 g of MG in 1000 mL of deionized water. Working solutions were obtained by serial dilution. The maximum absorption wavelength was confirmed at 621.6 nm using a UV–Visible spectrophotometer (Shimadzu UV-1800).

Effect of adsorbent dosage

Various masses of nano-hydrogel (0.006–0.06 g) were added to 10 mL of MG solution (500 mg/L) at pH 7 and 25°C. After shaking for 3 h, the residual MG concentration was measured spectrophotometrically.

Effect of contact time

The optimum dosage (0.008 g) was contacted with 10 mL of MG solution (500 mg/L) at pH 7 and 25°C for varying time intervals (1–150 min). Samples were withdrawn at predetermined times and analysed.

Effect of pH

The solution pH was varied from 2 to 10 using 1 M HCl or NaOH. The adsorbent (0.008 g) was added to 10 mL of MG solution (500 mg/L) and agitated at 120 rpm until equilibrium was reached.

The equilibrium adsorption capacity (q_e, mg/g) and removal efficiency (R%) were calculated using Eqs. 1 and 2:

$$q_e = (C_0 - C_e) \times V / m \quad (1)$$

$$R\% = [(C_0 - C_e) / C_0] \times 100 \quad (2)$$

where C_o and C_e (mg/L) are the initial and equilibrium concentrations, V (L) is the solution volume, and m (g) is the adsorbent mass.

Regeneration and Reusability Experiments

The reusability of the nano-hydrogel was evaluated over five consecutive adsorption–desorption cycles (n = 3 per cycle). In each cycle, 0.008 g of the nano-hydrogel was equilibrated with 10 mL of MG solution (500 mg/L, pH 7) at 25°C for 90 min. After adsorption, the supernatant was analysed spectrophotometrically to determine the residual MG concentration. The spent nano-hydrogel was then desorbed by immersion in 20 mL of 0.1 M HCl in 50% (v/v) ethanol and shaken at 150 rpm for 60 min. The desorbed nano-hydrogel was washed with deionized water until neutral pH, dried at 60°C for 12 h, and re-used in the next adsorption cycle. Desorption efficiency was calculated as the ratio of MG released during desorption to MG adsorbed during the preceding adsorption step × 100. All measurements were performed in triplicate, and the results are reported as mean ± standard deviation (SD). Statistical significance across cycles was assessed by one-way ANOVA at the 95% confidence level ($p < 0.05$).

Applicability in Real Water Matrices

To evaluate the practical applicability of the nano-hydrogel, adsorption experiments were conducted using four different water matrices: (i) deionized water (control), (ii) tap water (Al-Diwaniyah municipal supply; total dissolved solids, TDS ≈ 480 mg/L, pH 7.3), (iii) river water (collected from the Diwaniyah River; TDS ≈ 890 mg/L, pH 7.8, turbidity 18 NTU), and (iv) simulated industrial wastewater (prepared by supplementing deionized water with 100 mg/L Na^2SO^4, 50 mg/L NaCl, 20 mg/L $CaCl^2$, 10 mg/L humic acid, and 5 mg/L phenol, pH adjusted to 7.0). Each matrix was spiked with 500 mg/L MG, and adsorption was conducted under optimum conditions (0.008 g adsorbent, 90 min, 25°C). All experiments were performed in triplicate (n = 3). One-way ANOVA followed by Tukey's post-hoc test was used to compare qe values across matrices ($p < 0.05$).

RESULTS AND DISCUSSION

Characterization of the Nano-hydrogel

The FTIR spectrum of the synthesized nano-hydrogel confirmed the successful copolymerization and cross-linking. A broad absorption band centred at 3794 cm^{-1} was attributed to overlapping O–H and N–H stretching vibrations from pectin and NIPAm, respectively. Bands at 2925 and 2857 cm^{-1} corresponded to asymmetric and symmetric C–H stretching of

aliphatic chains. The carbonyl stretching band at 1730 cm^{-1} confirmed the presence of ester groups from acrylic acid and pectin, while the amide I band at 1600 cm^{-1} and amide II band at 1547 cm^{-1} verified the incorporation of NIPAm into the polymer network. Additional bands at 1458 cm^{-1} (CH_2 bending), 1258 cm^{-1} (C–O–C stretching), and 1024 cm^{-1} (C–O stretching of pectin sugar rings) further supported the composite structure [16,17].

The XRD pattern displayed a broad hump between 15° and 30° (2θ) with a diffuse peak at approximately 20.7°, characteristic of a semi-crystalline to amorphous polymeric material. This pattern is consistent with the disordered cross-linked network formed between pectin, PNIPAm, and polyacrylic acid chains [18]. The absence of sharp crystalline peaks confirmed that the nano-hydrogel matrix was predominantly amorphous.

FE-SEM micrographs revealed a folded sheet-

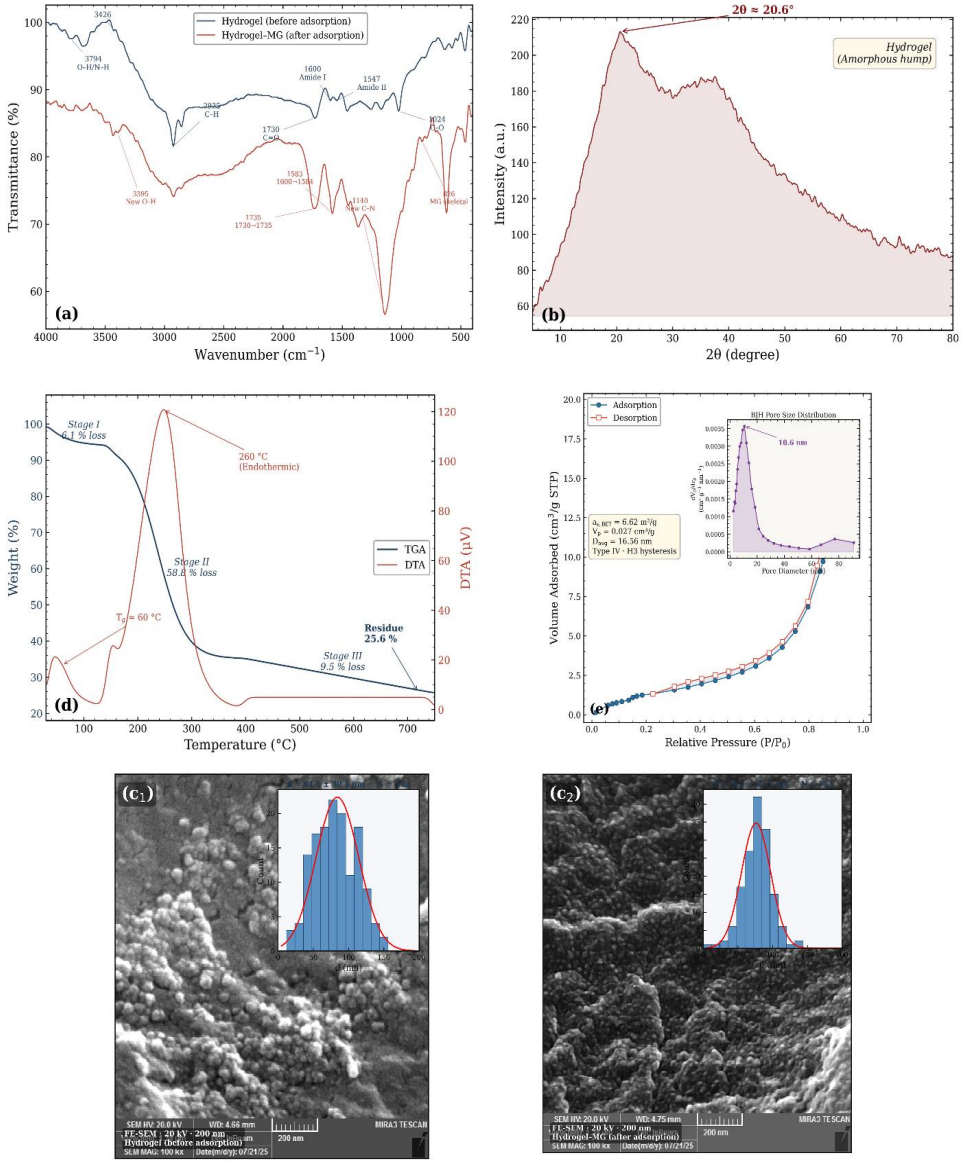

Fig. 2. Characterization of the pectin/poly(NIPAm-co-AA) nano-hydrogel: (a) FTIR spectra before and after malachite green adsorption, (b) XRD pattern, (c_1) FE-SEM micrograph with particle size distribution histogram before adsorption, (c_2) FE-SEM micrograph with particle size distribution histogram after MG adsorption, (d) TGA/DTA thermogram, and (e) BET nitrogen adsorption–desorption isotherm with BJH pore size distribution (inset).

like morphology with wrinkles and surface undulations typical of dried cross-linked hydrogels. Statistical analysis of 142 particulate features yielded a mean diameter of 84.1 nm (σ = 30.4 nm), with visible surface cavities and pores that serve as potential adsorption sites [19]. BET analysis showed a specific surface area of 6.62 m^2/g, a total pore volume of 0.027 cm^3/g, and an average pore diameter of 16.56 nm, classifying the material as mesoporous according to IUPAC nomenclature. The nitrogen adsorption–desorption isotherm followed a Type IV pattern with an H3 hysteresis loop, indicative of slit-shaped mesopores arising from stacked polymeric sheets [20]. TGA revealed three-stage weight loss: dehydration (30–150°C, 6.1%), organic decomposition (150–400°C, 58.8%), and advanced carbonization (400–750°C, 9.5%), with a total mass loss of 74.4% [21].

Effect of Adsorbent Dosage

The influence of adsorbent dosage on MG removal was investigated by varying the nano-hydrogel mass from 0.006 to 0.06 g while keeping other parameters constant (C_o = 500 mg/L, V = 10 mL, pH = 7, T = 25°C). As shown in Fig. 3a, the removal efficiency increased steadily from 86.90% at 0.006 g to essentially 100% at 0.06 g, which is logically attributed to the greater number of active binding sites available at higher dosages [22]. Conversely, the equilibrium adsorption capacity (q_e) declined from 724.13 to 83.33 mg/g over the same range, reflecting the underutilization of available sites when the adsorbent is present in excess relative to the quantity of solute molecules. Such behaviour is commonly reported in the literature and arises because, at elevated adsorbent loadings, a large fraction of binding sites remain unsaturated [23]. A dosage of 0.008 g was selected as the optimum working mass, as it provided a favourable balance between adsorption capacity (596.04 mg/g) and removal percentage (95.37%). This dosage was therefore employed in all subsequent experiments. All batch experiments throughout this study were performed in triplicate (n = 3), and results are expressed as mean ± standard deviation (SD) unless stated otherwise.

Effect of Contact Time and Equilibrium

The kinetics of MG adsorption onto the nano-hydrogel were studied at the optimum dosage (0.008 g) with a contact time ranging from 1 to 150 min (Fig. 3b). Three distinct phases were observed in the time-dependent adsorption profile. During the initial rapid uptake phase (0–10 min), the adsorption capacity rose sharply from 515.29 to 577.29 mg/g, corresponding to the immediate occupation of readily accessible surface sites by MG molecules through electrostatic attraction and hydrogen bonding. In the second phase (10–60 min), the rate of uptake decelerated progressively as the surface sites became increasingly saturated and diffusion into the interior pore network began to govern the process. Finally, an equilibrium plateau was attained between 60 and 90 min, with no statistically significant change in q_e beyond this interval (q_e = 604.89 mg/g, R% = 96.78%). The rapid initial uptake may be attributed to the strong electrostatic interaction between the cationic MG molecules and the deprotonated carboxyl groups ($–COO^-$) on the nano-hydrogel surface, which are abundant due to the acrylic acid and pectin components of the polymer network [24]. The existence of a clear equilibrium plateau confirms monolayer-to-multilayer transition saturation of the available binding sites [25].

Adsorption Kinetic Modelling

To gain mechanistic insights into the adsorption process, three kinetic models were applied in both linear and non-linear forms: the pseudo-first-order (PFO), pseudo-second-order (PSO), and Weber–Morris intraparticle diffusion models.

Table 1. Effect of adsorbent dosage on MG adsorption capacity and removal efficiency (C_o = 500 mg/L, V = 10 mL, pH = 7, T = 25°C).

Adsorbent dosage (g)	Ce (mg/L)	qe (mg/g)	R (%)
0.006	65.52	724.13	86.90
0.008	23.17	596.04	95.37
0.010	23.98	476.02	95.20
0.030	17.10	160.97	96.58
0.050	13.74	97.25	97.25
0.060	< LOD	83.33	100.00

Pseudo-First-Order Model

The Lagergren pseudo-first-order model assumes that the rate of change in solute uptake is directly proportional to the difference between the equilibrium capacity and the amount adsorbed at any given time. Its linearized form is expressed as:

$$\log(q_e - q_t) = \log q_e - (k_1/2.303)t \quad (3)$$

Although the PFO model yielded a reasonable regression coefficient (R^2 = 0.8596 for the linear form), the calculated equilibrium capacity (q_e,calc) deviated considerably from the experimental value (q_e,exp = 604.89 mg/g). This discrepancy is typical of systems in which chemisorption, rather than simple physisorption, governs the rate of uptake. The PFO model is generally applicable only to the initial stages of adsorption and tends to underperform when the process involves chemical bonding between the adsorbate and adsorbent surface [26].

Pseudo-Second-Order Model

The Ho and McKay pseudo-second-order model presumes that the overall rate of adsorption is controlled by chemisorption involving electron sharing or transfer between the adsorbate and active surface sites:

$$t/q_t = 1/(k_2 q_e^2) + t/q_e \quad (4)$$

The PSO model provided an excellent fit to the experimental data, with $R^2 \approx 1.000$ (RMSE = 0.89 mg/g, SSE = 10.61) for the linear regression. The calculated equilibrium capacity (q_e,calc = 605.13 mg/g) was in close agreement with the experimental value (604.89 mg/g), and the rate constant k_2 was determined as 3.654×10^{-3} g/mg·min (i.e., 0.003654 g/mg·min). The initial adsorption rate ($h = k_2 q_e^2 \times 10^{-6}$ g/mg·min. The initial adsorption rate ($h = k_2 q_e^2$) was calculated as 1338.14 mg/g·min, reflecting the strong affinity between MG molecules and the nano-hydrogel surface functional groups [27]. The dominance of the PSO model confirms that the adsorption of MG onto the nano-hydrogel is predominantly governed by chemisorption, involving electron-pair sharing between the nitrogen atoms in the MG structure and the carboxyl and amide groups on the polymer network, alongside electrostatic interactions between the cationic dye and the anionic surface [28].

Weber–Morris Intraparticle Diffusion Model

The Weber–Morris model was employed to assess the contribution of intraparticle diffusion to the overall rate:

$$q_t = k_i^d t^{1/2} + C \quad (5)$$

The plot of q_t versus $t^{1/2}$ exhibited two distinct linear segments, suggesting a multi-step

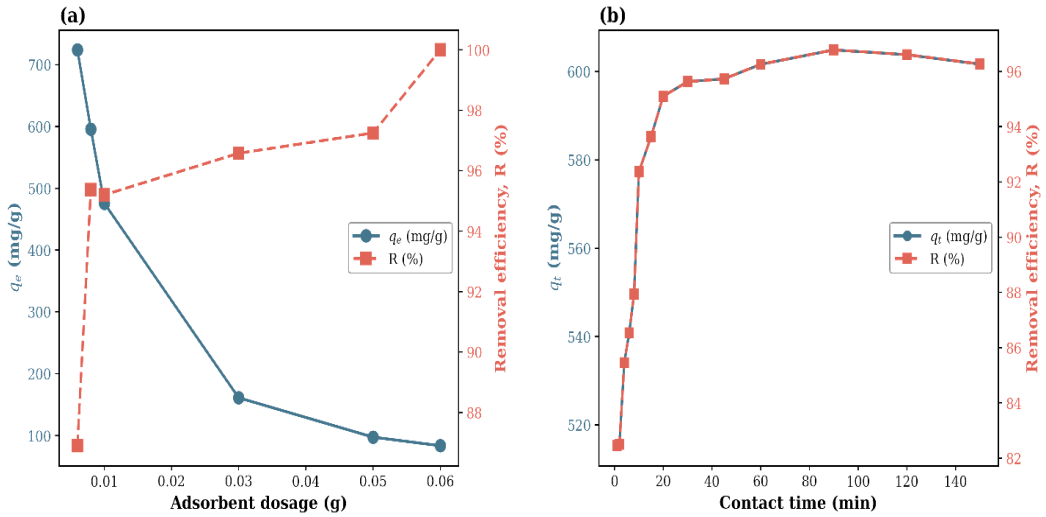

Fig. 3. (a) Effect of adsorbent dosage on adsorption capacity (q_e, left axis) and removal efficiency (R%, right axis); (b) Effect of contact time on adsorption capacity (q_t) and removal efficiency at optimal dosage (C_o = 500 mg/L, pH = 7, T = 25°C).

diffusion process. The first segment (k_i^d,1 = 26.49 mg/g·min$^{1/2}$) represented rapid external surface adsorption and boundary layer diffusion, while the second segment (k_i^d,2 = 1.67 mg/g·min$^{1/2}$) corresponded to the slower intraparticle diffusion within the mesoporous network of the nano-hydrogel. Importantly, the linear segments did not pass through the origin (C ≠ 0), which indicates that intraparticle diffusion was involved but was not the sole rate-limiting step. The non-zero intercept values suggest that boundary layer effects and chemical interactions at the surface also

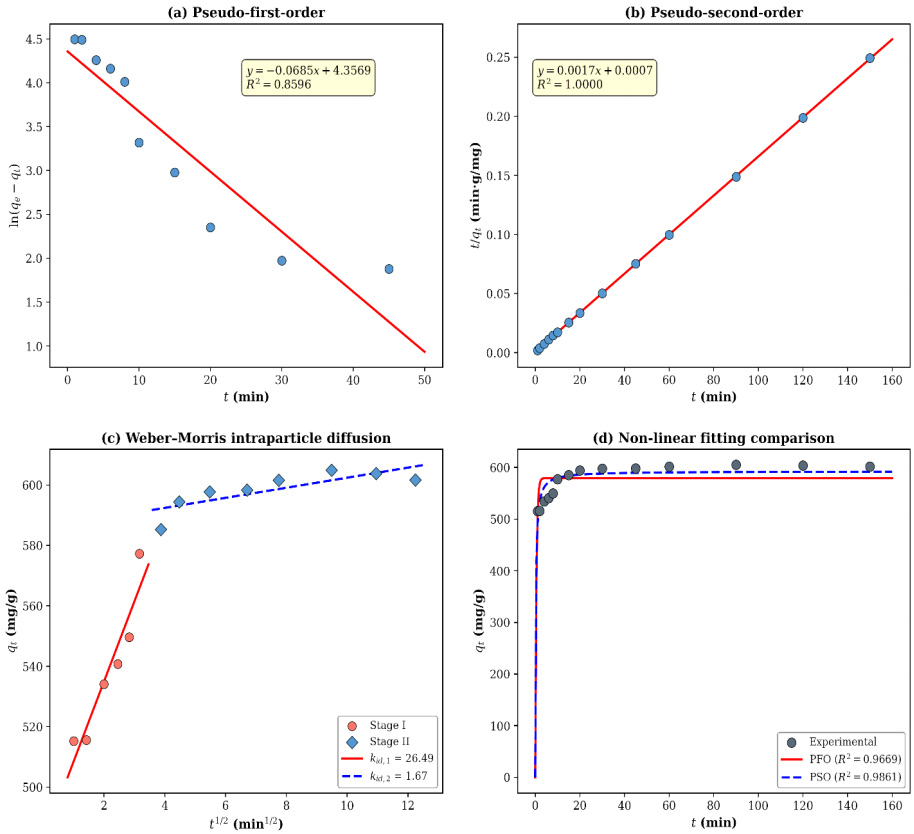

Fig. 4. Kinetic modelling of MG adsorption onto the nano-hydrogel: (a) pseudo-first-order linear plot, (b) pseudo-second-order linear plot, (c) Weber–Morris intraparticle diffusion plot, and (d) non-linear fitting comparison of PFO, PSO, and experimental data.

Table 2. Kinetic parameters for MG adsorption onto pectin/poly(NIPAm-co-AA) nano-hydrogel derived from PFO, PSO, and Weber–Morris models.

Model / Parameter	Unit	Linear	Non-linear
qe, exp (experimental)	mg/g	604.89	604.89
Pseudo-first-order (PFO)			
qe, calc	mg/g	78.02	579.22
k_1	min^{-1}	0.0685	1.9951
R^2	—	0.8596	0.9669
Pseudo-second-order (PSO)			
qe, calc	mg/g	605.13	592.43
k_2	g/mg·min	0.003654	0.007654
h (= $k_2 q_e^2$)	mg/g·min	1338.14	2686.32
R^2	—	1.0000	0.9861
Weber–Morris intraparticle diffusion		Stage I	Stage II
kid	mg/g·min$^{1/2}$	26.49	1.67
C (intercept)	mg/g	482.04	585.76
R^2	—	0.8949	0.6454

contributed significantly to the overall rate control [29]. This multi-step mechanism is consistent with the mesoporous structure revealed by BET analysis (average pore diameter = 16.56 nm), which provides pathways for gradual MG diffusion into the interior of the nano-hydrogel particles after the external surface sites are saturated [30].

Point of Zero Charge (pH_{p1t})

The point of zero charge is a fundamental parameter that dictates the surface charge of an adsorbent as a function of solution pH and consequently governs the electrostatic interactions between the adsorbent and ionic adsorbates. The pH drift results for the synthesized nano-hydrogel are presented in Fig. 5. The plot of ΔpH versus pH_i revealed that the pH_{PZC} was located at pH 4.2, which is the pH_i value at which ΔpH equals zero. At pH < 4.2, the ΔpH values were positive, indicating that the surface consumed protons from solution (i.e., the surface was positively charged). At pH > 4.2, the ΔpH values became negative, signifying proton release and a net negative surface charge [15].

The acidic pH_{PZC} value (4.2) is attributed to the abundance of carboxylic acid groups from two sources: acrylic acid (pKa ≈ 4.25) and galacturonic acid residues in pectin (pKa ≈ 3.5). At pH values above the pH_{PZC}, deprotonation of these carboxyl groups (–COOH → $–COO^-$ + H^+) generates a negatively charged surface that readily attracts cationic species such as MG through electrostatic attraction [31]. This finding is central to understanding the pH-dependent adsorption behaviour discussed in the following section.

Effect of Solution pH on MG Adsorption

The solution pH exerts a profound influence on adsorption performance by modulating both the surface charge of the adsorbent and the speciation of the dye in solution. Fig. 5 illustrates the variation of q_e with pH in the range 2–10. At pH 2, the lowest adsorption capacity was recorded (q_e = 515.21 mg/g, R% = 82.43%). This can be explained by the protonation of carboxyl and amide groups on the nano-hydrogel surface at pH values well below the pH_{PZC}, which renders the surface positively charged and creates electrostatic repulsion with the cationic MG molecules. Moreover, the high concentration of H^+ ions in strongly acidic media competes with MG cations for the limited negatively charged binding sites [32]. As the pH increased from 2 to 4, a noticeable improvement in q_e was observed, coinciding with the approach to the pH_{PZC} (4.2) where the surface transitions from a net positive to a net negative charge. Beyond pH 4, the progressive ionization of –COOH groups to $–COO^-$ significantly enhances the anionic character of the surface, thereby strengthening electrostatic attraction towards MG cations. Notably, q_e values remained high and relatively stable across the pH range 4–10 (592–609 mg/g), with the maximum

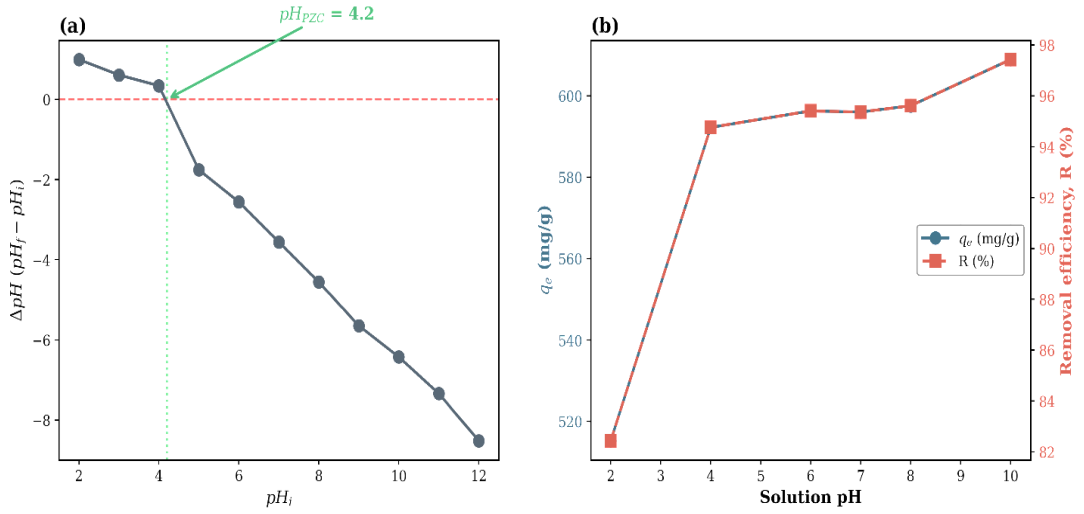

Fig. 5. (a) Determination of the point of zero charge (ΔpH vs. pH_i) for the nano-hydrogel (pH_{p1t} = 4.2); (b) Effect of solution pH on MG adsorption capacity (q_e) and removal efficiency (R%) at optimum conditions.

observed at pH 10 (q_e = 608.96 mg/g). This broad operational pH window is of considerable practical importance, as it indicates that the nano-hydrogel can function effectively without stringent pH control in real wastewater applications [33]. The pH dependence of adsorption also provides mechanistic information. The fact that a substantial removal (82.43%) was achieved even at pH 2—where the surface is positively charged—implies that non-electrostatic interactions such as hydrogen bonding between MG and the amide (–CONH–) and hydroxyl (–OH) groups of the nano-hydrogel, as well as π–π interactions involving the aromatic rings of MG and the polymer backbone, contribute meaningfully to the overall adsorption mechanism. At alkaline pH, the combination of electrostatic attraction, hydrogen bonding, and π–π stacking results in maximum uptake. These findings are corroborated by the FTIR analysis of the nano-hydrogel after MG adsorption, which revealed shifts in the O–H, C=O, and amide I bands, alongside the appearance of new peaks attributable to MG structural vibrations [34,35].

Regeneration and Reusability

The practical viability of any adsorbent is critically dependent on its regeneration potential and reusability over multiple cycles. Fig. 6 presents the adsorption capacity, removal efficiency, and desorption efficiency of the pectin/poly(NIPAm-co-AA) nano-hydrogel over five successive adsorption–desorption cycles using 0.1 M HCl in 50% ethanol as the eluent (n = 3 per cycle). The adsorption capacity decreased gradually from 604.89 ± 8.12 mg/g in the first cycle to 531.27 ± 12.64 mg/g in the fifth cycle, corresponding to a cumulative capacity retention of 87.8% (Fig. 6a). Similarly, the removal efficiency declined from 96.78 ± 1.30% to 85.00 ± 2.02%. One-way ANOVA confirmed that the decrease in qe across cycles was statistically significant ($F = 38.80$, $p < 0.001$), reflecting progressive loss of active sites due to irreversible chemisorption and structural relaxation of the polymer network [39]. The desorption efficiency also decreased from 94.32 ± 2.14% (cycle 1) to 82.67 ± 3.45% (cycle 5) (Fig. 6b), suggesting that a fraction of MG molecules are retained by strong covalent-like interactions (consistent with the PSO mechanism) that resist elution. Nonetheless, the retention of >85% of the initial adsorption capacity after five cycles compares favourably with other hydrogel-based adsorbents reported in the literature [40,41] and confirms the suitability of the nano-hydrogel for repeated use in practical water treatment scenarios.

Applicability in Real Water Matrices

The performance of the nano-hydrogel was further examined in four water matrices of

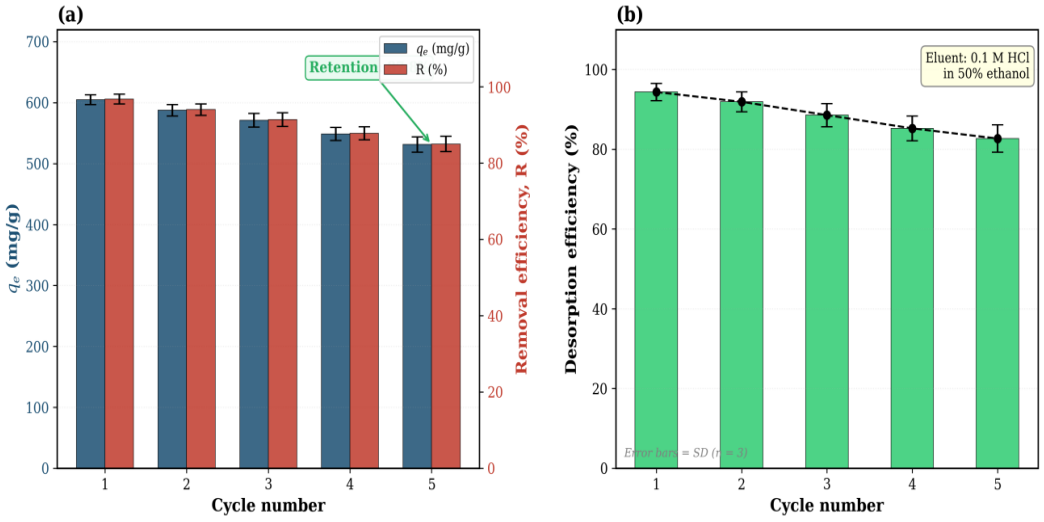

Fig. 6. Regeneration and reusability of the nano-hydrogel over five adsorption–desorption cycles (eluent: 0.1 M HCl in 50% ethanol; n = 3, error bars = SD): (a) adsorption capacity (qe) and removal efficiency (R%); (b) desorption efficiency per cycle.

increasing complexity to assess its tolerance to competing ions, natural organic matter (NOM), and other co-contaminants (Fig. 7). All experiments were conducted in triplicate (n = 3) under optimum conditions (C_o = 500 mg/L, 0.008 g, pH 7, 25°C, 90 min). In deionized water, the nano-hydrogel achieved qe = 604.89 ± 8.12 mg/g (R = 96.78 ± 1.30%). A modest reduction was observed in tap water (qe = 578.34 ± 10.67 mg/g, R = 92.53 ± 1.71%), attributable to the competitive adsorption of Ca^{2+} and Mg^{2+} ions that partially screen the anionic surface sites. In river water, the adsorption capacity decreased further to 552.17 ± 13.24 mg/g (R = 88.35 ± 2.12%), which can be ascribed to the

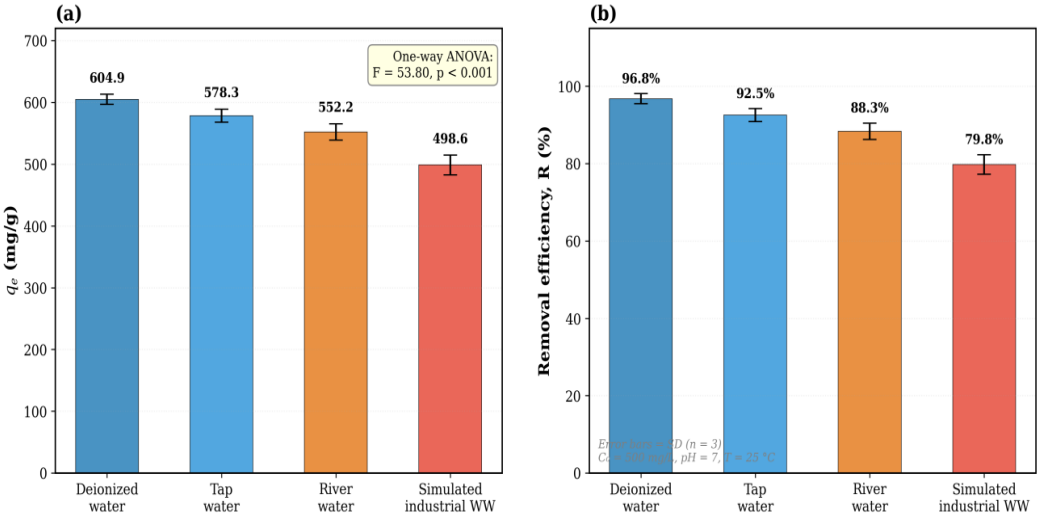

Fig. 7. Adsorption performance of the nano-hydrogel in different water matrices (C_o = 500 mg/L, 0.008 g, pH 7, 25 °C, 90 min; n = 3, error bars = SD): (a) adsorption capacity (qe); (b) removal efficiency (R%).

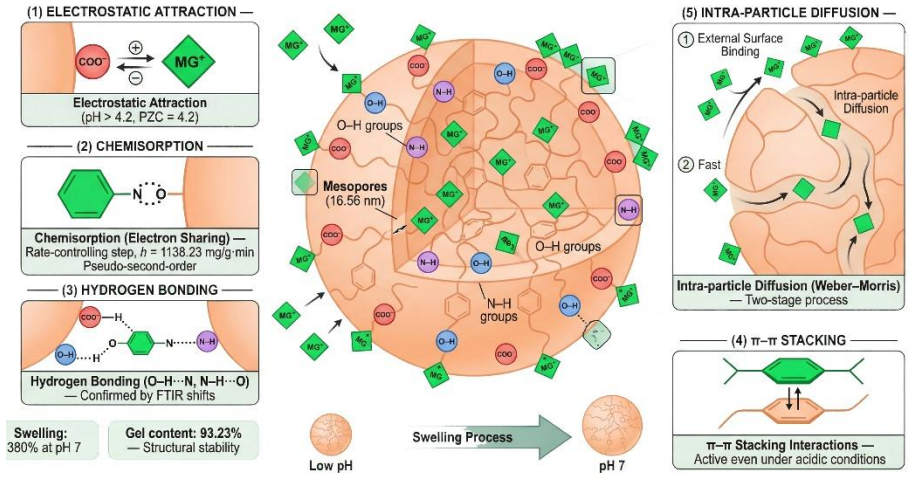

Fig. 8. Proposed adsorption mechanism of MG^+ onto pectin/poly(NIPAm-co-AA) nano-hydrogel showing the five interaction pathways: electrostatic attraction, chemisorption, hydrogen bonding, π–π stacking, and intra-particle diffusion, along with pH-responsive swelling behaviour.

combined effects of elevated TDS, NOM fouling of surface sites, and colloidal competition [42]. The most pronounced reduction occurred in simulated industrial wastewater (qe = 498.63 ± 15.89 mg/g, R = 79.78 ± 2.54%), where humic acid and phenol compete for hydrogen-bonding and π–π stacking sites, and the high ionic strength compresses the electrical double layer, diminishing electrostatic attraction [43]. One-way ANOVA revealed a statistically significant difference in qe across the four matrices ($F = 53.80$, $p < 0.001$). Tukey's post-hoc analysis indicated that the DI–river and DI–industrial pairs were significantly different ($p < 0.01$), whereas the DI–tap pair was not ($p = 0.078$). Despite the reductions observed in complex matrices, the nano-hydrogel retained >79% removal efficiency even in the most challenging medium, demonstrating its robustness for practical water treatment applications.

Mechanism

Based on the kinetic data, pH study, PZC determination, and FTIR evidence, a comprehensive adsorption mechanism can be proposed for MG uptake by the pectin/poly(NIPAm-co-AA) nano-hydrogel. At pH values above 4.2, the surface acquires a net negative charge due to the ionization of carboxylic groups from both acrylic acid and pectin, which facilitates strong electrostatic attraction with the positively charged MG molecules. The pseudo-second-order kinetics and the high initial adsorption rate (h = 1338.14 mg/g·min) indicate that electron sharing between MG nitrogen atoms and surface functional groups (chemisorption) is the rate-controlling step. The two-stage Weber–Morris profile reveals that after rapid external surface binding, MG molecules gradually diffuse through the mesopores (average diameter 16.56 nm) to access interior binding sites. The FTIR shifts confirm that hydrogen bonds form between O–H/N–H groups of the nano-hydrogel and the dye, while π–π stacking interactions between the aromatic MG rings and the polymer backbone contribute to adsorption even under acidic conditions where electrostatic repulsion would otherwise dominate [37,38]. The high gel content (93.23%) ensures structural stability during the swelling-mediated adsorption process, and the pH-responsive swelling (reaching 1380% at pH 7) enhances accessibility of internal binding sites.

CONCLUSION

A pectin/poly(NIPAm-co-acrylic acid) nano-hydrogel was successfully prepared by aqueous free-radical copolymerization and thoroughly characterized by FTIR, XRD, FE-SEM, TGA, and BET techniques. The synthesized nano-hydrogel demonstrated excellent adsorptive performance towards malachite green dye, achieving an equilibrium capacity of 604.89 mg/g and 96.78% removal at the optimum dosage of 0.008 g. The adsorption kinetics were best described by the pseudo-second-order model ($R^2 \approx 1.000$, RMSE = 0.89 mg/g), confirming that chemisorption is the dominant rate-controlling mechanism. The Weber–Morris analysis revealed a two-step diffusion process, with rapid surface adsorption followed by slower intraparticle diffusion, while the non-zero intercept ruled out intraparticle diffusion as the sole rate-limiting step. The pH study, supported by the determination of pH_{PZC} at 4.2, established that the surface carries a net negative charge at pH > 4.2, which promotes electrostatic attraction with the cationic MG molecules. The high and relatively constant adsorption capacity observed over the pH range 4–10 (592–609 mg/g) demonstrates the operational versatility of the nano-hydrogel. FTIR analysis after adsorption confirmed the involvement of electrostatic interactions, hydrogen bonding, and π–π stacking in the binding mechanism. Regeneration experiments confirmed that the nano-hydrogel retains 87.8% of its initial capacity after five cycles, while tests in real water matrices (tap, river, and simulated industrial wastewater) showed removal efficiencies of 92.53%, 88.35%, and 79.78%, respectively. These results collectively establish the pectin/poly(NIPAm-co-AA) nano-hydrogel as a promising, reusable, eco-friendly, and pH-responsive adsorbent for the efficient removal of cationic dyes from industrial wastewater, with demonstrated robustness for real-world water treatment applications.

ACKNOWLEDGEMENTS

The authors gratefully acknowledge the University of Al-Qadisiyah for providing laboratory facilities and support for this research.

CONFLICT OF INTEREST

The authors declare that there is no conflict of interests regarding the publication of this

manuscript.

REFERENCES

1. Said TO, Ragab S, El Sikaily A, Arshad M, Hassaan MA, Yılmaz M, et al. Characterization and health risk assessment of n-alkanes and PAHs in sediments from Shalateen (Halayeb Triangle), Egyptian Red Sea Coast. Environ Pollut. 2024;363:125203.
2. Xu Z, Zada N, Habib F, Ullah H, Hussain K, Ullah N, et al. Enhanced Photocatalytic Degradation of Malachite Green Dye Using Silver–Manganese Oxide Nanoparticles. Molecules. 2023;28(17):6241.
3. Al-Tohamy R, Ali SS, Li F, Okasha KM, Mahmoud YAG, Elsamahy T, et al. A critical review on the treatment of dye-containing wastewater: Ecotoxicological and health concerns of textile dyes and possible remediation approaches for environmental safety. Ecotoxicology and Environmental Safety. 2022;231:113160.
4. Ritter MT, Lobo-Recio MÁ, Padilla I, Nagel-Hassemer ME, Romero M, López-Delgado A. Adsorption of Safranine-T dye using a waste-based zeolite: Optimization, kinetic and isothermal study. Journal of Industrial and Engineering Chemistry. 2024;136:177-187.
5. Rashid R, Shafiq I, Akhter P, Iqbal MJ, Hussain M. A state-of-the-art review on wastewater treatment techniques: the effectiveness of adsorption method. Environmental Science and Pollution Research. 2021;28(8):9050-9066.
6. Al-Ghouti MA, Da'ana DA. Guidelines for the use and interpretation of adsorption isotherm models: A review. J Hazard Mater. 2020;393:122383.
7. Ahmed EM. Hydrogel: Preparation, characterization, and applications: A review. Journal of Advanced Research. 2015;6(2):105-121.
8. Bashir S, Hina M, Iqbal J, Rajpar AH, Mujtaba MA, Alghamdi NA, et al. Fundamental Concepts of Hydrogels: Synthesis, Properties, and Their Applications. Polymers. 2020;12(11):2702.
9. Schild HG. Poly(N-isopropylacrylamide): experiment, theory and application. Prog Polym Sci. 1992;17(2):163-249.
10. Guo X, Liu H, Nail A, Meng D, Zhu L, Li C, et al. Design and Application of Stimuli-Responsive Nanocomposite Hydrogels: A Review. Macromol Rapid Commun. 2025;46(12).
11. Gnanasambandam R. Determination of pectin degree of esterification by diffuse reflectance Fourier transform infrared spectroscopy. Food Chem. 2000;68(3):327-332.
12. Weerasundara L, Gabriele B, Figoli A, Ok Y-S, Bundschuh J. Hydrogels: Novel materials for contaminant removal in water—A review. Crit Rev Environ Sci Technol. 2020;51(17):1970-2014.
13. Lu Q, Zheng J, Yu J, Yang S, Ma D, Yang W, et al. Synthesis and Adsorption Properties for Cationic Dyes of Acrylic Acid/Vermiculite Hydrogel Initiated by Glow-Discharge-Electrolysis Plasma. Adv Polym Tech. 2016;37(4):996-1007.
14. Makhado E, Pandey S, Nomngongo PN, Ramontja J. Preparation and characterization of xanthan gum-cl-poly(acrylic acid)/o-MWCNTs hydrogel nanocomposite as highly effective re-usable adsorbent for removal of methylene blue from aqueous solutions. Journal of Colloid and Interface Science. 2018;513:700-714.
15. Kosmulski M. Surface Charging and Points of Zero Charge: CRC Press; 2009 2009/05/14.
16. Guthrie RD. Introduction to Spectroscopy (Pavia, Donald; Lampman, Gary M.; Kriz, George S., Jr.). J Chem Educ. 1979;56(10):A323.
17. Barth A. Infrared spectroscopy of proteins. Biochim Biophys Acta. 2007;1767(9):1073-1101.
18. Preparation and Characterization of Acid Resistant Double Cross-Linked Hydrogel for Potential Biomedical Applications. American Chemical Society (ACS). http://dx.doi.org/10.1021/acsbiomaterials.7b00818.s001
19. Guilherme MR, Aouada FA, Fajardo AR, Martins AF, Paulino AT, Davi MFT, et al. Superabsorbent hydrogels based on polysaccharides for application in agriculture as soil conditioner and nutrient carrier: A review. Eur Polym J. 2015;72:365-385.
20. Sing KSW, Everett DH, Haul RAW, Moscou L, Pierotti RA, Rouquérol J, et al. Experimental Procedures. IUPAC Standards Online: De Gruyter; 2016. http://dx.doi.org/10.1515/iupac.57.0011
21. Ghasri M, Bouhendi H, Kabiri K, Zohuriaan-Mehr MJ, Karami Z, Omidian H. Superabsorbent polymers achieved by surface cross linking of poly(sodium acrylate) using microwave method. Iranian Polymer Journal. 2019;28(7):539-548.
22. Hameed B, Din A, Ahmad A. Adsorption of methylene blue onto bamboo-based activated carbon: Kinetics and equilibrium studies. J Hazard Mater. 2007;141(3):819-825.
23. Ofomaja AE. Intraparticle diffusion process for lead(II) biosorption onto mansonia wood sawdust. Bioresour Technol. 2010;101(15):5868-5876.
24. Crini G. Non-conventional low-cost adsorbents for dye removal: A review. Bioresour Technol. 2006;97(9):1061-1085.
25. Wang J, Guo X. Adsorption isotherm models: Classification, physical meaning, application and solving method. Chemosphere. 2020;258:127279.
26. Revellame ED, Fortela DL, Sharp W, Hernandez R, Zappi ME. Adsorption kinetic modeling using pseudo-first order and pseudo-second order rate laws: A review. Cleaner Engineering and Technology. 2020;1:100032.
27. Ho YS, McKay G. Pseudo-second order model for sorption processes. Process Biochem. 1999;34(5):451-465.
28. Ho Y. Review of second-order models for adsorption systems. J Hazard Mater. 2006;136(3):681-689.
29. Weber WJ, Morris JC. Kinetics of Adsorption on Carbon from Solution. Journal of the Sanitary Engineering Division. 1963;89(2):31-59.
30. Perkins D. Euan Cameron, The European Reformation. 2nd Ed. Oxford/New York/Auckland, Oxford University Press 2012 Cameron Euan The European Reformation. 2nd Ed. 2012 Oxford University Press Oxford/New York/Auckland £ 24,99. Historische Zeitschrift. 2013;296(1):196.
31. Frimmel FH. Chemistry of the Solid-Water Interface. Processes at the Mineral-Water and Particle-Water Interface in Natural Systems. Von W. Stumm. Wiley, Chichester, 1992. X, 428 S., Broschur 32.50 £ - ISBN 0–471–57672–7. Angew Chem. 1993;105(5):800-800.
32. Mall ID, Srivastava VC, Agarwal NK, Mishra IM. Adsorptive removal of malachite green dye from aqueous solution by bagasse fly ash and activated carbon-kinetic study and equilibrium isotherm analyses. Colloids Surf Physicochem Eng Aspects. 2005;264(1-3):17-28.
33. Yang H, Wu K, Zhu J, Lin Y, Ma X, Cao Z, et al. Highly efficient and selective removal of anionic dyes from aqueous solutions using polyacrylamide/peach gum polysaccharide/

attapulgite composite hydrogels with positively charged hybrid network. Int J Biol Macromol. 2024;266:131213.
34. Saha TK, Bhoumik NC, Karmaker S, Ahmed MG, Ichikawa H, Fukumori Y. Adsorption of Methyl Orange onto Chitosan from Aqueous Solution. Journal of Water Resource and Protection. 2010;02(10):898-906.
35. Srivastava S, Sinha R, Roy D. Toxicological effects of malachite green. Aquat Toxicol. 2004;66(3):319-329.
36. Hameed BH, El-Khaiary MI. Malachite green adsorption by rattan sawdust: Isotherm, kinetic and mechanism modeling. J Hazard Mater. 2008;159(2-3):574-579.
37. Zhao H, Xie M, He S, Lin S, Wang S, Liu X. Development of a Novel Nanoclay-Doped Hydrogel Adsorbent for Efficient Removal of Heavy Metal Ions and Organic Dyes from Wastewater. Gels. 2025;11(4):287.
38. Zhang Z, Lu Y, Gao S, Wu S. Sustainable and Efficient Wastewater Treatment Using Cellulose-Based Hydrogels: A Review of Heavy Metal, Dye, and Micropollutant Removal Applications. Separations. 2025;12(3):72.
39. Alcalde-Garcia F, Prasher S, Kaliaguine S, Tavares JR, Dumont M-J. Desorption Strategies and Reusability of Biopolymeric Adsorbents and Semisynthetic Derivatives in Hydrogel and Hydrogel Composites Used in Adsorption Processes. ACS Engineering Au. 2023;3(6):443-460.
40. Makhado E, Pandey S, Modibane KD, Kang M, Hato MJ. Sequestration of methylene blue dye using sodium alginate poly(acrylic acid)@ZnO hydrogel nanocomposite: Kinetic, Isotherm, and Thermodynamic Investigations. Int J Biol Macromol. 2020;162:60-73.
41. Abu Elella MH, Aamer N, Abdallah HM, López-Maldonado EA, Mohamed YMA, El Nazer HA, et al. Novel high-efficient adsorbent based on modified gelatin/montmorillonite nanocomposite for removal of malachite green dye. Sci Rep. 2024;14(1).
42. Lv A, Lv X, Xu X, Shao Z-B. Tailored ultra-tough, antimicrobial and recyclable hydrogels based on chitosan and ionic liquid modified montmorillonite with different chain lengths for efficient adsorption of organic dyes in wastewater. Int J Biol Macromol. 2024;257:128752.
43. Ebrahimi S, Zanganeh P, Nouripour-Sisakht S, Javadian H, Babaie A, Khaleghi R, et al. A multifunctional graphene oxide–ZnO nanohybrid for rapid and highly efficient malachite green adsorption and strong broad-spectrum antimicrobial activity. Sci Rep. 2026;16(1).